An empirical approach to develop near-field limit for radiated-emission compliance check

See, Kye Yak; Fang, Ning; Wang, Lin-Biao; Soh, Weishan; Svimonishvili, Tengiz; Oswal, Manish; Chang, Weng-Yew; Koh, Wee-Jin

2014

See, K. Y., Fang, N., Wang, L. B., Soh, W., Svimonishvili, T., Oswal, M., et al. (2014). An empirical Approach to develop near-field limit for radiated-emission compliance check. IEEE transactions on electromagnetic compatibility, 56(3), 691-698.

https://hdl.handle.net/10356/105192

https://doi.org/10.1109/TEMC.2014.2302003

An Empirical Approach to Develop Near-Field Limit for Radiated-Emission Compliance Check

Kye-Yak See, *Senior Member, IEEE,* Ning Fang, Lin-Biao Wang, Weishan Soh, Tengiz Svimonishvili, Manish Oswal, *Member, IEEE,* Weng-Yew Chang, *Senior Member, IEEE,* and Wee-Jin Koh, *Senior Member, IEEE*

***Abstract*—Based on measurements from a near-field scanner and far-field measurements obtained in a semi-anechoic chamber, a statistical relationship is established between a magnetic field in the near field and an electric field in the far field. The relationship makes it possible to transform a radiated-emission regulatory limit from the far-field to the near-field zone. The transformed near-field limit can allow efficient prediction of radiated-emission compliance for high-speed printed circuit boards. The presented results demonstrate the feasibility of the proposed method for a quick radiated-emission pre-compliance check without heavy equipment investment.**

***Index Terms*—Electromagnetic compatibility (EMC), empirical approach, far-field (FF)-to-near-field (NF) limit transformation, radiated emissions.**

I. Introduction

THE rising clock frequencies during the past decade have increased the likelihood of high-speed printed circuit boards (PCBs) failing radiated-emissions tests for electromagnetic compatibility (EMC) compliance. With intense market competition, product designers face increased pressure to develop radiated-emission compliant PCBs within a very tight product development schedule. Therefore, the availability of radiated-emission measurement facilities and EMI troubleshooting capabilities is crucially important.

A straightforward way to verify that a PCB has complied with a regulatory EMC requirement is to measure its emission in a semi-anechoic chamber (SAC) or a gigahertz transverse electromagnetic (GTEM) cell; the measured emission level is then compared with the standard regulatory limit directly [1]. SAC is widely used for radiated-emission measurements, but it can be costly and occupies a significant amount of "real estate." In contrast, GTEM cell is less bulky and relatively inexpensive. Still, it is not widely recognized as a fully compliant test setup and is usually used for pre-compliance radiated-emission test purposes. Although both SAC and GTEM can be used for a radiated-emission compliance check, neither measurement setup enables designers to effectively and rapidly identify the cause of EMI failure to implement EMC countermeasures.

A near-field (NF) electromagnetic (EM) scanner is an efficient tool capable of locating the sources of significant radiation from a PCB. Even though the NF scanner is more compact and less expensive than both SAC and GTEM, it does not indicate whether a PCB will comply with the far-field (FF) radiated-emission limit. Hence, it would be beneficial to circuit designers if the NF scanner were to provide such information. Much research has been done to predict the FF radiated emission using the NF measurement data. For instance, in [2]-[5] equivalent surface currents are computed across the whole surface area of a PCB. Reference [6] takes into consideration multiple reflections from objects near the device under test. In addition to the amplitude information, the approach in [6] requires the NF emission phase information, which is crucial for predicting the FF emission accurately through equivalent surface currents. The phase information is usually determined by using two NF probes or from bi-planar NF measurements by solving the free space Green function [7].

To predict the FF radiated emission from the NF measurement data, [8]-[11] use a genetic algorithm to find the radiation sources of a device from NF measurements. References [12] and [13] involve the deduction of sets of equivalent dipoles and loops from measured NF patterns. The sets of equivalent dipoles and loops cumulatively emit EM fields (similar to those measured in NF), which are used to calculate the radiated emission from a PCB in the FF region. Even though the phase retrieval using the actual NF data works well for very simple PCB structures, it is difficult to implement for PCBs with complex digital circuit layouts. Furthermore, the wide emission frequency range and frequency-dependent radiation patterns add to the complexity of the FF emission prediction. Thus, numerical modeling involving various approaches in [2]-[13] will be extremely costly and, most likely, unfeasible for the FF radiated emission prediction over a wide frequency range.

The objective of this paper is to establish a NF emission limit for a PCB from a FF radiated-emission limit given in an EMC standard. The proposed method combines experiment and theory to obtain a relationship between the FF radiated electric field and NF magnetic field. The relationship makes it possible to transform the regulatory FF emission limit to

Manuscript received April 19, 2012; revised August 21, 2013 and December 3, 2013; accepted January 7, 2014. This work was fully supported by the Defense Science and Technology Agency (DSTA), Singapore, under the Defense Innovative Research Program (DIRP).

K.-Y. See and T. Svimonishvili are with the School of Electrical and Electronic Engineering, Nanyang Technological University, Singapore 639789 (e-mail: EKYSEE@ntu.edu.sg; TENGIZ.S@ntu.edu.sg).

N. Fang is with the School of Electronics and Information Engineering, Beijing University of Aeronautics and Astronautics, Beijing 100191, China (e-mail: fangn31@163.com).

L.-B. Wang is with Continental Automotive Singapore Pte Ltd, Singapore 339780 (e-mail: lin.biao.wang@continental-corporation.com).

W. Soh is with the Halliburton Completion Tools Manufacturing Pte Ltd, Singapore 637131 (e-mail: Weishan.Soh@halliburton.com).

M. Oswal is with the Hewlett Packard, Singapore 109683 (e-mail: MOSWAL@ieee.org).

W.-Y. Chang and W.-J. Koh are with the DSO National Laboratories, Singapore 118230 (e-mail: CWENGYEW@dso.org.sg; KWEEJIN@dso.org.sg).

the NF limit for a quick and inexpensive compliance check. Encouraging results presented in this paper demonstrate the feasibility of the proposed method for such a check.

II. Description of the Proposed Method

A. NF Regulatory Limits

The more complex PCBs are, the more computationally challenging it is to accurately quantify dipoles and loops for the prediction of radiated fields. Moreover, computer modeling becomes prohibitive for high-speed PCBs made of hundreds and thousands of interconnects with complex layouts. The maximum NF H-field produced by a given PCB is usually due to a dominant source or "hot spot" at a specific location on the PCB surface. Hence, as a first-order approximation, the "hot spot" can be treated as a virtual loop antenna to predict the FF E-field of the PCB at each emission frequency.

The arrangement in Fig. 1 shows a complex PCB with

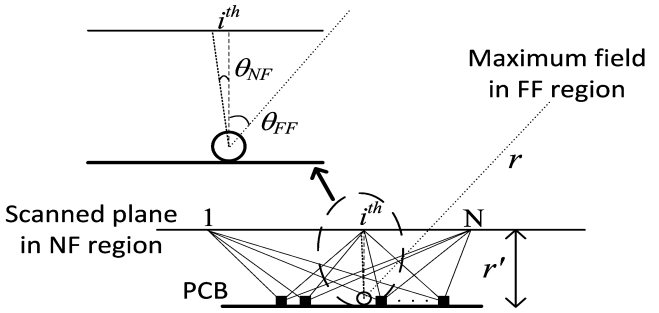

Fig. 1. Relationship between the PCB and the virtual loop antenna. The inset shows NF and FF angles.

multiple emission sources (squares) and a virtual loop antenna ("hot spot") denoted by an open circle. Using a NF EM scanner, the radiated NF magnetic field from the emission sources is recorded at points 1 through N at a constant height r' above the surface of the PCB. The scanned area extends 10 mm beyond the PCB surface in both x and y directions, which, based on our experience, is sufficient to detect and measure the NF H-field from all parts of the PCB surface. Since the magnitude of the measured field is a function of position and direction, a rational position is selected for compliance estimation. In Fig. 1, the NF H-field maximum occurs at the i^{th} point and the H-field there is given by

$$|H(f)|_{\text{NF, max}} = \max_i(\sqrt{|H_{x,i}(f)|^2 + |H_{y,i}(f)|^2 + |H_{z,i}(f)|^2} \quad (1)$$

where $H_{x,i}$, $H_{y,i}$, and $H_{z,i}$ are the NF H-field components along the x, y, and z axes, respectively. f in (1) is electromagnetic wave frequency. The location on the PCB directly under the i^{th} point is designated and modeled as a virtual loop antenna to predict the maximum FF E-field of the PCB.

Considering a small circular loop antenna of radius a, the total H-field in the NF zone is given by [14]

$$|H|_{\text{NF}} \approx \frac{a^2 I_0}{2r'^3} \cos\theta_{\text{NF}} \quad (2)$$

where the spatial current I_0 is a constant. The angle θ_{NF} is measured from the axis that is normal to the plane of the loop and passes through its center. Equation (2) assumes that θ_{NF} is negligible, which means that $\sin\theta_{\text{NF}} \approx 0$. Using [14] and (2), the FF E-field for the same circular loop antenna reads

$$|E|_{\text{FF}} \approx \left(\frac{k^2 r'^3}{2r}\right)\left\{\frac{\sin\theta_{\text{FF}}}{\cos\theta_{\text{NF}}}\right\}\eta|H|_{\text{NF}} \quad (3)$$

where $k = 2\pi/\lambda$, λ is the free-space wavelength at frequency f, η is the free-space impedance, and r is the distance from the center of the virtual loop antenna to a field point in the FF region.

Defining an angle transfer function, $A(f)$, such that

$$A(f) = \frac{\sin\theta_{\text{FF}}}{\cos\theta_{\text{NF}}} \quad (4)$$

and solving (3) for $|H|_{\text{NF}}$, we get

$$|H|_{\text{NF}} \approx \frac{2r}{A(f)\eta k^2 r'^3}|E|_{\text{FF}}. \quad (5)$$

Equation (5) allows the FF E-field to be transformed to the NF H-field. If $|E|_{\text{FF}}$ is a regulatory limit in the FF zone, then $|H|_{\text{NF}}$ in (5) will represent a regulatory limit in the NF zone. This means that the numeric value of $|H|_{\text{NF}}$ at each frequency will be the largest allowable magnetic field magnitude in the NF region. A compliance check for a given PCB in the NF region can be done by comparing $|H|_{\text{NF}}$ from (5) with the maximum NF H-field of the PCB obtained from a NF EM scanner. Since the NF EM scanner only measures the magnitude of the NF H-field, the disadvantage of the proposed approach is that no phase information is included in calculations. In (5), the transfer function $A(f)$ can be obtained statistically by recording both the FF E-field and NF H-field at each frequency. This is discussed in the next subsection.

B. Determination of Transfer Function

Since an electromagnetic field can vary markedly (by two, three orders of magnitude) across the surface of a complex PCB, our interest is in determining the logarithm (logarithm to the base 10) of the angle transfer function. As will be shown in the next section, in this paper we deal with a small sample, n = 14, whose underlying distribution's variance is unknown. By assuming a normal population distribution, which is a reasonable assumption even in the case of moderate deviation from normality, we can easily estimate a confidence interval (CI) on the mean of $\log_{10} A$ population from the mean and variance of $\log_{10} A$ sample. Since many populations are well approximated by a normal distribution, this approach has an added advantage of being more widely applicable [15]. Rearranging (5), the logarithm of A is

$$\log_{10} A \approx \log_{10}\left(\frac{2r}{k^2 r'^3}\right) + \log_{10}\left(\frac{|E|_{\text{FF}}}{\eta|H|_{\text{NF}}}\right). \quad (6)$$

To determine if (6) is distributed normally, the values of $\log_{10} A$ at each frequency are first grouped together as one set of sampled data p, which is discussed in the next section. Next, a probability plot is used to see if the computed values conform to a normal distribution. To generate a normal probability

plot, the data are arranged in ascending order and then plotted against their percent cumulative frequency, which is given by

$$100\left(\frac{l-0.5}{n}\right)\% \tag{7}$$

where l is the rank of the sampled data and n is the number of data points. If the data points approximately follow a straight line drawn through them, then the normal distribution is an appropriate model for the sampled data [15]. A 100(1-α)% CI on the mean, μ, of the assumed normal $\log_{10} A$ population with unknown variance reads

$$\mu = \bar{p} \pm t_{\alpha/2,n-1}\frac{\hat{s}}{\sqrt{n}} \tag{8}$$

where $\bar{p}$ and $\hat{s}^2$, the mean and variance of the sampled data p, are given by

$$\bar{p} = \frac{1}{n}\sum_{i=1}^{n} p_i \tag{9}$$

$$\hat{s}^2 = \frac{1}{n-1}\sum_{i=1}^{n}(p_i - \bar{p})^2 \tag{10}$$

and $t_{\alpha/2,n-1}$ in (8) is tabulated and represents the upper $100\alpha/2$ percentage point of the t distribution with $n-1$ degrees of freedom [15].

It should be noted that distributions other than the normal one are often necessary to statistically describe a given set of experimental data. For instance, in [16] experimental data are analyzed by plotting their probability plots against several theoretical distributions such as the Weibull, generalized extreme value, exponential, inverse Gaussian, Birnbaum-Saunders, log-normal, and log-logistic. Also, practical problems in engineering and science frequently involve non-deterministic relationships between two or more variables, which requires a different collection of statistical tools such as, for example, the linear regression [17].

III. Characterization of Boards

This section starts with a discussion of NF and FF measurement setups. The maximum NF magnetic, $|H|_{\text{NF, max}}$, and FF electric, $|E|_{\text{FF, max}}$, field emission profiles are measured for 14 multilayer boards, the number of layers ranging from 2 to 8. The boards are designed to operate at three different clock frequencies, namely 10 MHz, 25 MHz, and 50 MHz. At the end of the section, we examine the statistical characteristics of $\log_{10} A$.

A. NF Measurements

Fig. 2 shows a measurement setup for the NF scanning system. The system consists of an EM scanner (Detectus RS321, 100 kHz to 3 GHz) [18], including a positioner and NF probes, and a spectrum analyzer (SA) (ROHDE & SCHWARZ FSL6, 9 kHz to 6 GHz) for frequency domain measurements. Since PCBs are relatively thin, and can be regarded as two-dimensional structures, the scanning operation is performed parallel to the PCB surface. In Fig. 2, the PCB is parallel to the XY-plane. The NF probe attached to the positioner moves in steps of 10 mm along the scanning plane to measure

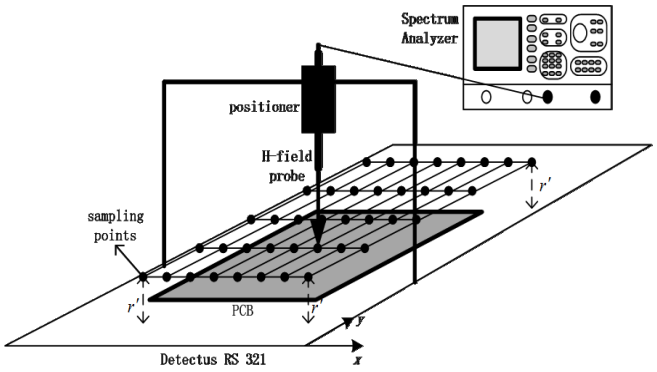

Fig. 2. Setup for obtaining the NF emission profile using the Detectus EM Scanner.

the magnetic field components $|H_{x,i}|$, $|H_{y,i}|$, and $|H_{z,i}|$. The SA records the probe output and converts it to absolute field intensities.

In Fig. 2, the distance r' between the magnetic field probe and PCB is set to 10 mm and is chosen such that $kr' < 1$, which approximately defines the NF region. The $|H|_{\text{NF, max}}$ is recorded from 30 MHz to 1 GHz with the SA detector function set to a quasi-peak mode. The SA resolution bandwidth (RBW) is 120 kHz in compliance with the minimum FCC bandwidth of 120 kHz.

B. FF Measurements

For every PCB, the electric field in the FF region is measured in SAC at a height of 80 cm from the ground plane with a tri-log antenna placed 3 m away from the PCB. The FF E-field is recorded from 30 MHz to 1 GHz with the measurement receiver function in a quasi-peak mode and the receiver RBW set to 120 kHz. During the measurement procedure, the antenna height is scanned from 1 m to 4 m in both horizontal and vertical polarizations. In addition, every PCB is placed at three orthogonal axes and at each axis the PCB is rotated through 360 degrees. This is to maximize emissions with the highest amplitude relative to the imposed radiated emission limit so that $|E|_{\text{FF, max}}$ is obtained for each emission frequency.

C. Angle Transfer Function

To generate a set of sampled data p for $\log_{10} A$ (Subsection II-B), $|E|_{\text{FF, max}}$ and $|H|_{\text{NF, max}}$ (obtained from SAC and NF scanner as described in Subsections III-A and III-B) are substituted into (6) along with the values of k, r, r', and η at 15 frequencies ranging from 50 MHz to 500 MHz at 50 MHz intervals and from 500 MHz to 1000 MHz at 100 MHz intervals. Since there are 14 PCBs, each set of sampled data p consists of 14 data points at each of the 15 frequencies.

Fig. 3 and Fig. 4 show normal probability plots of $\log_{10} A$ at 100 MHz, 300 MHz, 500 MHz, and 800 MHz. As can be seen in the figures, the data approximately follow the straight lines drawn through them. In addition, considering a small sample size of merely 14 PCBs, the data points do not deviate severely from linearity. Moreover, the data points pass the "fat

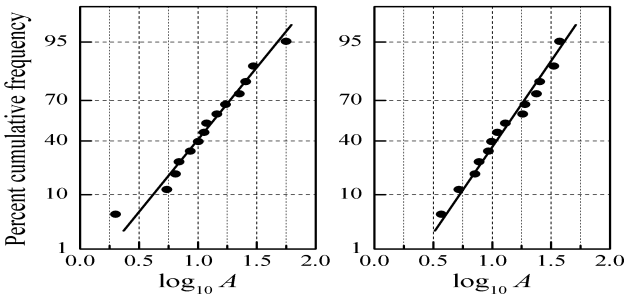

Fig. 3. Normal probability of $\log_{10} A$ at 100 MHz (left) and 300 MHz (right).

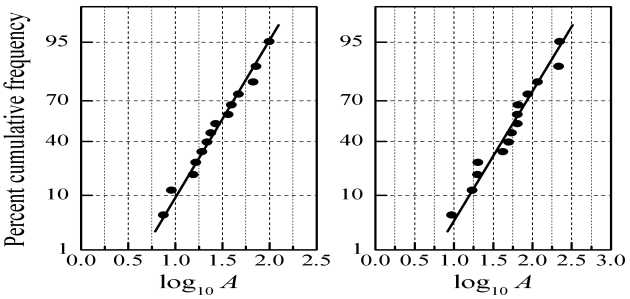

Fig. 4. Normal probability of $\log_{10} A$ at 500 MHz (left) and 800 MHz (right).

pencil" test, which leads us to conclude that the logarithm of the angle transfer function A is normally distributed [15].

The logarithm of A as a function of frequency is plotted in Fig. 5, where the open symbols are the values of $\log_{10} A$ for each of the 14 PCBs. The solid symbols (stars) in Fig. 5 are computed from (9) and represent the mean of $\log_{10} A$. Also, the solid vertical lines, given by (8), show the upper and lower bounds for a 90% CI constructed around the mean. From an

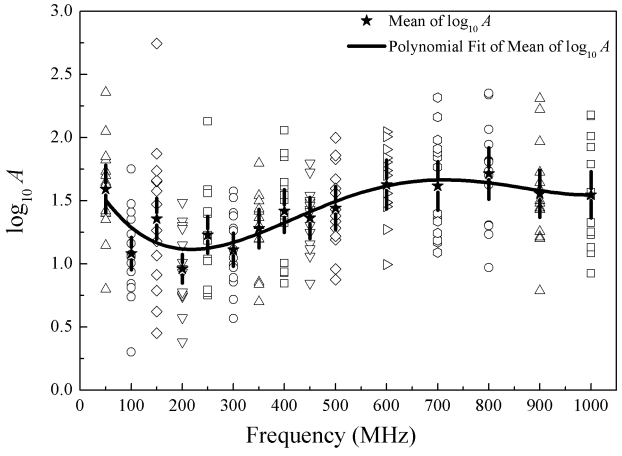

Fig. 5. Variation of $\log_{10} A$ (open symbols) and the mean of $\log_{10} A$ (solid stars) with frequency.

EMC design perspective, the upper bound is more critical than the lower one because it predicts the worst possible emission from a newly designed board. If the predicted worst case emission is either below or very close to the regulatory EMI limit, there is a high likelihood of the board complying with the regulatory limit.

Our goal in this paper is to compute $|H|_{\text{NF, max}}$ from (5) so that we can establish a NF emission limit for PCBs from the FF radiated-emission limit given in an EMC standard. To do that, we need to be able to express the mean of $\log_{10} A$ as a function of frequency. By fitting 2nd through 5th degree polynomials to the mean of $\log_{10} A$ (while varying the number of significant figures in the polynomial coefficients from two to five) and using an R squared statistic to measure the goodness of fit, we conclude that the 4th degree polynomial yields the best fit to the mean of $\log_{10} A$. Hence, the variation of the mean of $\log_{10} A$ with frequency is approximated by the 4th degree polynomial (solid curve in Fig. 5) whose equation is given by

$$\log_{10} A = 1.837 - 7.940 \times 10^{-3} \times f + 2.782 \times 10^{-5} \times f^2 - 3.306 \times 10^{-8} \times f^3 + 1.289 \times 10^{-11} \times f^4. \quad (11)$$

Because none of the quantities on the right-hand side of (6) are measured manually, we assume that $\log_{10} A$ and, thus, the polynomial coefficients in (11) can have at least four significant figures. The formula in (11) is valid provided f lies within the range 50 MHz $\leq f \leq$ 1 GHz. To calculate $|H|_{\text{NF, max}}$, (5) is rearranged and manipulated to yield

$$|H|_{\text{NF, max}} \approx \frac{1}{10^{\left[\log_{10} A - \log_{10}\left(\frac{2r}{k^2 r^3}\right)\right]}} \frac{|E|_{\text{FF, max}}}{\eta} \quad (12)$$

where $|H|_{\text{NF, max}}$ has units A/m and $\log_{10} A$ in the denominator is given by (11). Note that varying the number of significant figures in the polynomial coefficients of (11) from three to five has a negligible effect on $|H|_{\text{NF, max}}$ in (12): the variation of $|H|_{\text{NF, max}}$ is less than 1% up to 800 MHz, eventually increasing to approximately 1.7% at 1 GHz. With $|E|_{\text{FF, max}}$ fixed, $|H|_{\text{NF, max}}$ decreases as f increases from 50 MHz to 1 GHz. We use (12) in the next section for two previously untested boards to predict their compliance with the FCC Class B limit for a quasi-peak detector in the measurement receiver [19].

IV. Prediction and Validation

To validate the proposed FF-to-NF limit transformation discussed in Section II, we evaluate and apply (12) (converted to dB (μA/m)) to two new high-speed boards designated Board I and Board II. Both boards consist of two layers. Also, Board I operates at a 25-MHz clock frequency, whereas Board II has a ground plane and operates at a 10-MHz clock frequency. The two boards are shown in Fig. 6.

The contour plots in Fig. 7 show the spatial variation of the total H-field for Boards I and II. The vertical and horizontal axes are the board length and width in mm. Also, the legends next to the plots display the H-field magnitude in units of dB (μA/m).

The data in Fig. 7 are recorded with the NF scanner at 150 MHz. The plots show the board areas ranging from low to high in emission intensity, the dashed rectangles enclosing regions with the highest level of emission. As a first-order approximation, as it can be seen in the figure, measuring the

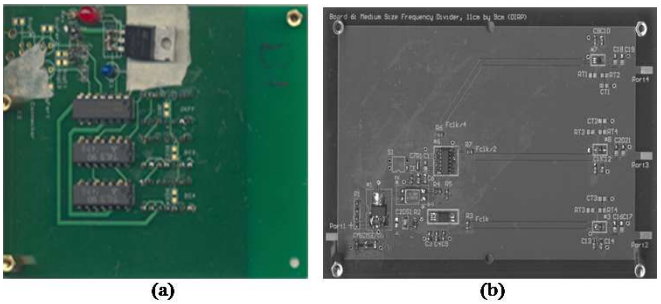

Fig. 6. Two high-speed prototypes: (a) Board I. (b) Board II.

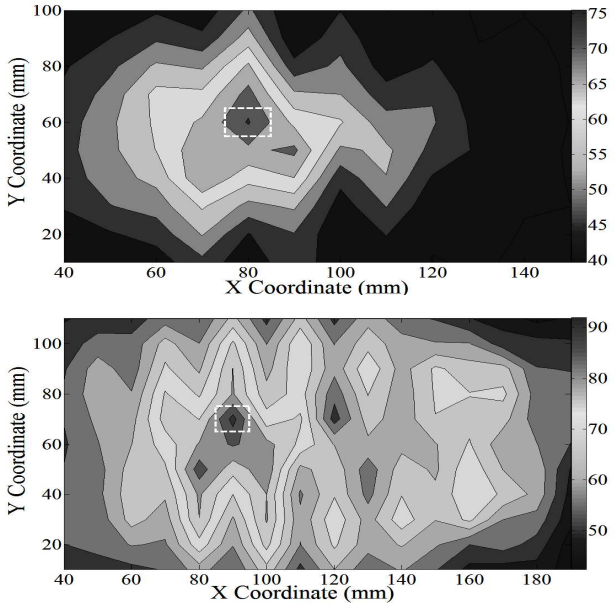

Fig. 7. Contour plots of NF H-field for Board I (top) and Board II (bottom) measured at 150 MHz.

field directly above the plane of the two PCBs should be sufficient to provide an estimation of their EMC performance.

For circuit designers, a convenient way to check compliance with the FCC Class B limit is to compare a measured field magnitude in the NF region with some useful criterion expressed in terms of the electromagnetic field strength. Fig. 8 shows the maximum magnetic field intensity for Boards I (solid circles) and II (open triangles) over the frequency range 30 MHz $\leq f \leq$ 1000 MHz. The data points are obtained from the NF scanner as described in Section III. The solid and dashed curves represent the transformed FCC Class B limit, $|H|_{\text{NF, max}}$, from (12), where $|E|_{\text{FF, max}}$, tabulated in [19], is the FCC Class B limit for a quasi-peak detector in the measurement receiver. Also, the solid curve in Fig. 8 is obtained by substituting (11) into (12), whereas the dashed curves are determined by substituting (for $\log_{10} A$) the upper and lower limits of the 90% CI for (11) into (12).

The compliance criterion in the NF region is that the emission field will pass the standard FCC Class B limit in the FF region provided the measured maximum NF H-field does not exceed the transformed FCC Class B limit. As can be seen in Fig. 8, the NF H-field magnitude for Board I is less

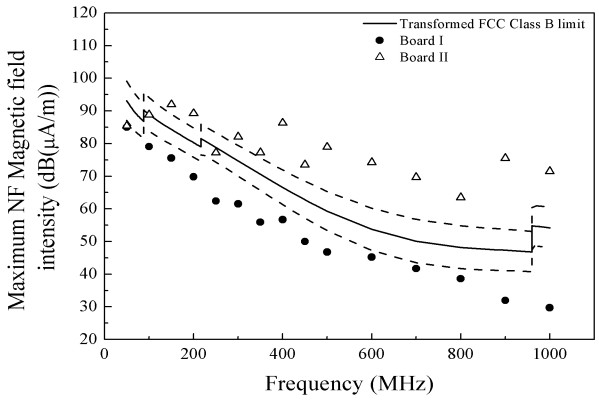

Fig. 8. Maximum NF H-field for Board I (solid circles) and Board II (open triangles). The solid curve is the transformed FCC Class B limit from (12).

than both the transformed FCC Class B limit and the lower bound over the frequency range shown. By contrast, the NF H-field magnitude for Board II exceeds both the transformed FCC Class B limit and the upper bound at all frequencies except 50 MHz, 100 MHz, and 250 MHz. Hence, based on the NF compliance criterion, we can expect Board I to comply with the FF FCC Class B limit over the entire frequency range and Board II to be out of compliance with the same limit over most of the frequency range shown in Fig. 8.

Displayed in Fig. 9 is the maximum FF E-field as a function of frequency for Boards I (lower plot) and II (upper plot). The FF E-field is measured in SAC as described in Section III. The solid line in both plots is the regulatory FCC Class B limit in the FF zone for a quasi-peak detector in the measurement receiver [19].

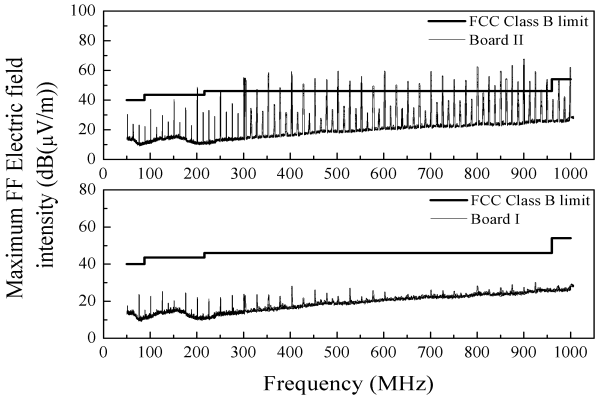

Fig. 9. Maximum FF E-field for Board I (lower plot) and Board II (upper plot).

As we can see in Fig. 9, the FF E-field for Board I is below the regulatory line, which means that Board I complies with the FCC limit over the entire frequency range. This is consistent with our observation in Fig. 8, where the data for Board I also lie below the transformed FCC Class B limit. In contrast to Board I, as can be seen in Fig. 9, Board II fails to comply with the FCC limit for frequencies greater than or equal to 200 MHz, which again agrees with the data for

Board II in Fig. 8. The foregoing discussion shows that (12) can predict the compliance (noncompliance) of Boards I and II with the standard FCC Class B limit given their compliance (noncompliance) with the transformed FCC Class B limit in the NF zone. Hence, the proposed method has the potential to be a simple and relatively inexpensive EMC pre-compliance tool.

Note that there are a few discrepancies between the data in Fig. 8 and 9. Even though the FF E-field for Board I is well below the regulatory line in Fig. 9, the same is not necessarily true of the NF H-field for Board I in Fig. 8. If the lower bound is selected as the transformed FCC Class B limit, as can be seen in Fig. 8, then the compliance of Board I with the NF regulatory limit is marginal at 50 MHz. Likewise, Board II is compliant in the FF zone for frequencies less than 200 MHz (Fig. 9). By contrast, as we can see in Fig. 8, it is not compliant at 150 MHz even if the upper bound is taken as the transformed FCC Class B limit. The observed overestimation and underestimation are partially due to the lack of NF phase information in the proposed method. Other potential contributing factors are the size, number of layers, operational speed, and measurement frequencies of Boards I and II.

V. Conclusion

To supplement existing EMC compliance tools, this paper proposes an approach that establishes a NF emission limit for PCBs from the FF radiated-emission limit given in an EMC standard. The described approach combines experiment and theory to obtain a relationship between the FF radiated electric field and NF magnetic field. The relationship, which takes advantage of statistics, transforms the regulatory FF emission limit to the NF limit for a quick and relatively inexpensive compliance check.

The method is applied to two, two-layer PCBs with 10- and 25-MHz clock frequencies. It is shown that the derived relationship successfully predicts the compliance (noncompliance) of the boards with the FF FCC Class B limit (for a quasi-peak detector in the measurement receiver) given their compliance (noncompliance) with the transformed FCC Class B limit in the NF zone. Hence, the proposed method has the potential to be a simple and relatively low-cost EMC pre-compliance tool. Moreover, it can eliminate the need for complex and time-consuming numerical modeling in some cases. It should be noted that the presented approach lacks phase information, which is partially responsible for overestimation and underestimation observed at several measurement frequencies. Therefore, future efforts will need to focus on incorporating both the magnitude and phase information into the proposed approach to make it more accurate, reliable, and robust.

The approach presented in the paper is based on 14 PCBs (with the number of layers ranging from 2 to 8) whose clock frequencies are 10 MHz, 25 MHz, and 50 MHz. Further studies, involving PCBs based on other technologies, are necessary to determine if the derived transfer function always conforms to a normal distribution and if the 14 PCBs (which is a small sample) used are representative of the entire PCB population.

Acknowledgment

The authors would like to acknowledge the research grant from DSTA under the Defense Innovative Research Program (DIRP).

References

[1] *American National Standard for methods of measurement of radio-noise emissions from low-voltage electrical and electronic equipment in the range of 9 kHz to 40 GHz*, ANSI Standard C63.4–2009.

[2] P. Petre and T. K. Sarkar, "Planar Near-Field to Far-Field Transformation using an Equivalent Magnetic Current Approach," *IEEE Trans. Antennas Propag.*, vol. 40, no. 11, pp. 1348–1356, Nov. 1992.

[3] T. K. Sarkar and A. Taaghol, "Near-Field to Near/Far-Field Transformation for Arbitrary Near-Field Geometry Utilizing an Equivalent Electric Current and MoM," *IEEE Trans. Antennas Propag.*, vol. 47, no. 3, pp. 566–573, Mar. 1999.

[4] Y. Vives, C. Arcambal, A. Louis, F de Daran, P. Eudeline, and B. Mazari, "Modeling Magnetic Radiations of Electronic Circuits using Near-field Scanning Method," *IEEE Trans. Electromagn. Compat.*, vol. 49, no. 2, pp. 391–400, Aug. 2007.

[5] P. -A. Barriere, J. -J. Laurin, and Y. Goussard, "Mapping of Equivalent Currents on High-Speed Digital Printed Circuit Boards Based on Near-Field Measurements," *IEEE Trans. Electromagn. Compat.*, vol. 51, no. 3, pp. 649–658, Aug. 2009.

[6] H. Weng, D. G. Beetner, and R. E. DuBroff, "Prediction of Radiated Emissions Using Near-Field Measurements," *IEEE Trans. Electromagn. Compat.*, vol. 53, no. 4, pp. 891–899, Nov. 2011.

[7] S. Gregson, J. McCormick, and C. Parini, *Principles of planar near-field antenna measurements*, 1st ed. London: The Institution of Engineering and Technology, pp. 296–303, 2007.

[8] J. -R. Regue, M. Ribo, J. -M. Garrell, S. Sorroche, and J. Ayuso, "A Genetic Algorithm Based Method for Predicting Far-Field Radiated Emissions from Near-Field Measurements," *IEEE Int. Symp. Electromagn. Compat.*, Washington DC, pp. 147–151, Aug. 2000.

[9] J. -R. Regue, M. Ribo, J. -M. Garrell, and A. Martin,"A Genetic Algorithm based Method for Source Identification and Far-Field Radiated Emissions Prediction from Near-Field Measurements for PCB Characterization," *IEEE Trans. Electromagn. Compat.*, vol. 43, no. 4, pp. 520–530, Nov. 2001.

[10] H. Fan and F. Schlagenhaufer, "Investigation of Near Field Data Sampling Approaches for Far Field Radiation Prediction of PCBs by Genetic Algorithm," *18th International Zurich Symposium on Electromagn. Compat.*, Munich, pp. 21–24, Sept. 2007.

[11] H. Fan and F. Schlagenhaufer, "Influence of planar sampling techniques of near field magnitude-only data on predicting far field radiation of PCBs by Genetic Algorithms," *IEEE Int. Symp. Electromagn. Compat.*, pp. 501–504, Jul. 2010.

[12] Q. Chen, M. Hangai, and K. Sawaya, "Estimation of Current Distribution by Near-Field Measurement," *in Proc. of the CEEM 2003, Asia Pacific Conference on Environmental Electromagnetics*, Hangzhou, China, pp. 482–485, Nov. 2003.

[13] J. Shi, M.A. Cracraft, J. Zhang, R.E. DuBroff, K. Slattery, and M. Yamaguchi, "Using Near-Field Scanning to Predict Radiated Fields," in *Proc. IEEE Int. Symp. Electromagn. Compat.*, Santa Clara, USA, vol. 1, pp. 14–18, Aug. 2004.

[14] C. A. Balanis, *Antenna Theory Analysis and Design*, 2nd ed. New York: Wiley, pp. 241–242, 1997.

[15] D. C. Montgomery and G. C. Runger, *Applied Statistics and Probability for Engineers*, 4th ed. New York: John Wiley & Sons, pp. 262–264, 2007.

[16] A. Mariscotti, A. Marrese, N. Pasquino, R. Schiano lo Moriello,"Time and Frequency Characterization of Radiated Disturbance in Telecommunication Bands due to Pantograph Arcing," *Measurement*, vol. 46, no. 10, pp. 4342–4352, Dec. 2013.

[17] M. D'Apuzzo, M. D'Arco, N. Pasquino,"Design of Experiments and Data-Fitting Techniques applied to Calibration of High-Frequency Electromagnetic Field Probes," *Measurement*, vol. 44, no. 6, pp. 1153–1165, Jul. 2011.

[18] *Detectus RS321 EMC Scanner User Manual*, Detectus AB, Malung, Sweden, 2011, pp. 35–66.

[19] *Title 47, Part 15, Subpart B: Unintentional Radiators*, Electronic Code of Federal Regulations, 2013.

Kye-Yak See (SM'02) received the B.Eng. degree with first class honors from the National University of Singapore, Singapore, in 1986 and the Ph.D. degree from Imperial College, London, U.K., in 1997, both in electrical engineering.

He is currently an Associate Professor in the School of Electrical and Electronic Engineering, Nanyang Technological University, Singapore. He also holds concurrent appointments of Head of the Circuits and Systems Division and Director of Electromagnetic Effects Research Laboratory. Prior to his academic career, he worked eight years in the industry, five years as Head of the Electromagnetic Compatibility (EMC) Centre, Singapore Technologies Electronic, and another three years as Lead EMC Design Engineer in ASTEC Custom Power, Singapore. His research interests are in the areas of computational electromagnetics, EMC design for power electronics, signal integrity issues for high-speed design and EMC measurement techniques. Dr. See is the founding Chair of the IEEE Singapore EMC Chapter and a Member of Singapore Technical Committee of EMC. He is also the Organizing Committee Chair for the 2006 and 2008 EMC Zurich Symposiums in Singapore. He has been a Technical Editor of IEEE EMC Magazine since January 2012.

Ning Fang was born on December 31, 1979, in Anshan, Liaoning Province, China. She received the B.S. and the Ph.D. degrees from the school of Electronic and Information Engineering from Beihang University, Beijing, China, in July 2002 and July 2007, respectively.

She is currently working with School of Electronics and Information Engineering, Beijing University of Aeronautics and Astronautics, Beijing, China.

Lin-Biao Wang (SM'11) received the B.Eng. and M.Sc. degrees in electrical and electronic engineering from Nanyang Technological University (NTU), Singapore, in 2006 and 2009, respectively. He is currently working toward his Ph.D. degree at NTU under the guidance of Prof. See Kye Yak.

He is currently working as a signal integrity engineer in Continental Automotive, Singapore. His research interests include electromagnetic interference (EMI) reduction techniques, frequency selective shielding, EMI/SI/PI modeling and high speed measurement techniques.

Weishan Soh received the B.Eng. and M.Sc. degrees in electrical and electronics engineering from Nanyang Technological University (NTU), Singapore, in 2008 and 2013, respectively.

During this period, she worked as a Research Engineer at Electromagnetic Effects Research Laboratory, NTU, Singapore. Her research work includes signal integrity and high-speed A/D converter designs. She is currently with Halliburton Completion Tools Manufacturing Pte Ltd, Singapore, as a Procurement Specialist Associate.

Tengiz Svimonishvili received the B.S. degree in physics from Tbilisi State University, Tbilisi, Republic of Georgia, in 1994, the M.S. degree in electrical engineering from the University of New Mexico (UNM), Albuquerque, NM, USA, in 2002, and the Ph.D. degree in engineering from UNM, Albuquerque, in 2011.

His dissertation work, the theory and particle-in-cell simulations of a compact THz source, was a collaborative effort between UNM and the High-Power Electrodynamics Group at the Los Alamos National Laboratory, Los Alamos, NM, USA. He is currently a Research Fellow in the School of Electrical and Electronic Engineering, Nanyang Technological University (NTU), Singapore. His research interests include THz sources, particle-in-cell simulations, and electromagnetic compatibility.

Manish Oswal (M'04) received the B.Eng. degree in electrical engineering from National University of Singapore, Singapore, in 2003 and the M.Eng. degree in electrical engineering from Nanyang Technological University (NTU), Singapore, in 2008.

After receiving the B.Eng. degree, he worked at NTU as a Research Engineer. He has worked in defense funded and joint projects with overseas universities in the field of electromagnetic compatibility (EMC). In addition, he has provided EMC consultation to the customers in the private and public sectors. He is currently a Senior Engineer with Hewlett Packard, Singapore. His main research interests include EMC and communication engineering.

Weng-Yew Chang (SM'12) received the Diploma degree (EEE, Merit) from Ngee Ann Polytechnic, Singapore, in Mar 1987. He received the B.Eng., M.Sc. and Ph.D. degrees from Nanyang Technological University (NTU), Singapore, in 1994, 2001, and 2011, respectively.

He joined DSO National Laboratories (formally Defence Science Organisation) in 1994. He began his career as a Hardware Designer under the Weapon Electronics Lab where he was involved in the development of an airborne embedded digital processing system. Subsequently, he became the Project Lead in numerous hardware de signs involving embedded DSP digital systems and airborne radar digital system. He last held the appointment of Group Head for Airborned Radar Digital Electronics Team under the division of Guided Systems before his Ph.D. study. He is currently a System Engineer for several new projects in 2012 in the area for high-speed computational intensive and ruggedized embedded modules for new generations of airborne digital systems. His research interests include signal integrity for high speed digital circuit design, high-speed measurements, practical techniques in design for EMI/EMC consideration, and ruggedized airborne embedded high-speed digital electronics systems design. He has co-authored more than 17 technical papers published in international referenced journals and conference proceedings.

Dr. Chang was awarded the Defense Technology Prize (Team Award) in 2000 and 2011. He was also awarded the DSO Group Performance Award in 2004 for contribution in Radar System. He was awarded a DSO scholarship in Dec 2005 to pursue his Ph.D. degree in NTU

Wee-Jin Koh (SM'03) received the B.Sc. degree from the Institute of Science and Technology, University of Manchester,Manchester, U.K., in 1979, the M.Sc. degree from the Naval Postgraduate School, Monterey, CA, USA, in 1987, and the Ph.D. degree from Ohio State University, Columbus, OH, USA, in 1995, all in electrical engineering.

Since 1981, he has been with DSO National Laboratories, Singapore. He has been an Adjunct Associate Professor in Nanyang Technological University (NTU), Singapore, since 2005. His research interests include EMI/EMC, lightning, and general EM.